Journal of the Korean Physical Society (2021) 78:210–218
https://doi.org/10.1007/s40042-020-00019-5

Online ISSN 1976-8524
Print ISSN 0374-4884

ORIGINAL PAPER

Long-range interactions in model colloidal dispersions with surface charge distributions

Seanea Jang[1] · **Ghi Ryang Shin**[1]

Received: 16 September 2020 / Accepted: 2 November 2020 / Published online: 18 December 2020

Abstract
The theoretical model, which is based on the density functional approach, has been developed for studying the electrostatic properties of colloidal dispersions (modified colloidal primitive model; MCPM) containing hard-spherical ions with a homogeneous surface charge distribution. The mean-spherical approximation for the multi-component charged ions has been used to account for the electrostatic ion correlation effects. The present study reflects the importance of the charge distribution of macroion in determining the ionic structure and mean forces acting on the macroions. Compared with the MCPM, the colloidal primitive model (CPM), on which the colloidal charge is assumed to be in the center of particle, shows very long-range electrostatic properties and mean force acting on the macroions because of the strong cross correlation between the hard-sphere contribution and the Coulomb interaction. The long-range attractions and repulsions in the charged colloidal dispersions originate from the entropic effects and are found at high packing fractions of the colloidal ions.

Keywords Colloidal dispersions · Modified colloidal primitive model · Density functional approach · Long-range effective interaction

1 Introduction

The study of colloidal and nanoparticle interactions and their interfacial properties is a major subject in the fields of physics, chemistry, biology, energy and technology [1–4]. Most studies on colloidal dispersions have been restricted to isolated macroion, i.e., infinite dilution or two liked-charged macroions immersed in a model electrolyte, with a focus on the electrolyte structure and electrostatic properties of colloidal dispersions, where phenomena such as charge reversal, charge inversion and overcharging have been shown to be relevant. However, experimental studies on colloidal dispersions at finite volume exhibit interesting phenomenology, which implies very long-range correlations. An example is polymer latex solutions in which an order-disorder structure of macroions [5–9], which cannot be explained in terms of conventional direct short-range interaction potentials, is observed.

Theoretical and simulation investigations of colloidal suspensions at finite volume fractions are difficult due to the large increase in the integration space for theoretical equations and the huge number of particles in larger simulation boxes because the charge distribution of a macroion has to be included in the theoretical model itself [10–18]. Lozada-Cassou et al. [19–22] recently proposed a theoretical model based on the hypernetted-chain/mean-spherical approximation (HNC/MSA) for studying the structural and the electrostatic properties of colloidal dispersions by using the modified colloidal primitive mode (MCPM), in which the charge of the macroion is uniformly smeared over its surface. They compared the results with those obtained using the colloidal primitive model (CPM) [20–22], in which the charge of a colloidal particle is assumed to be at its center for a local particle density and a mean force acting on the macroions. However, the CPM and the MCPM based on the HNC/MSA have shown the same particle distribution function and mean force between macroions in spite of different charge distribution of macroion. The charge distribution of macroions is known to be strongly affected by the mean forces between microions, as well as the local particle distribution functions

✉ Seanea Jang
seaneajang@gmail.com

Ghi Ryang Shin
gshin@anu.ac.kr

[1] Department of Physics, Andong National University, Andong 36729, Korea

[17, 18, 23]. On the other hand, the theoretical model of Lozada-Cassou et al., in some sense, does not satisfy self-consistency in itself; i.e., they calculated the local charge for the macroions from the local particle density and solved the Poisson equation to obtain the mean electrostatic potential arising from the spherical charge distribution of ions. Furthermore, to the best of our knowledge, no theoretical model satisfying self-consistency in itself has been used to study the structural and the electrostatic properties of the MCPM. Jang et al. [17, 18, 23] more recently proposed a theoretical model for studying the structural properties of size-symmetric electrolytes containing uniformly charged macroions, where the ions are treated as charged hard-sphere ions with a homogeneous charge distribution. They showed that the proposed model describes the simulation results well even for electrolytes with a high valence and that the particle density distributions of electrolytes depended strongly on the charge distributions of ions, as well as the attractive interactions between like-charged electrodes. We here extend the theoretical model in order to study a colloidal suspension with a charge distribution and investigate the long-range electrostatic properties and mean forces acting on the macroions at a finite colloidal concentration. We show that the charge distribution of macroions is suspected to play an important role in determining the ionic structure and the mean forces acting on the macroions.

In this paper, we will develop a theoretical model, the MCPM, for studying the structural properties of colloidal dispersions containing uniformly charged hard-sphere ions. In Sect. 2, we introduce the density functional approach based on the modified fundamental-measure theory (MFMT) for the hard-sphere contribution and the mean-field approximation for the cross interaction between the hard-sphere contribution and the Coulomb interaction. In Sect. 3, we compare the results obtained using the proposed theory with the Monte Carlo (MC) simulation results for the CPM model at a finite colloidal concentration. We show that long-range charge reversal and overcharging, as well as long-range mean forces of a uniformly charged colloidal suspension, are the results of intra-ionic correlations and finite colloidal concentrations. In concluding remarks, we briefly discuss the advantage of the proposed density functional approach and its future applications.

2 Model and theory

We consider three species of charged ions, i.e., positive ions, negative ions, and macroions of species denoted by +, −, and M, immersed in a solvent that is considered to be a medium of uniform dielectric permittivity ϵ [19, 21]. The macroions are assumed to be hard-sphere ions with a homogeneous surface charge density $\sigma = eZ_{\rm M}/\pi {d_{\rm M}}^2$, where e is the electronic charge, $Z_{\rm M}$ the valence, and $d_{\rm M}$ the diameter of macroions. The sizes of small ions (anions and counterions), each with a point charge embedded at the center of its sphere, which is much smaller than the sizes of macroions, are taken to be equal, $d_+ = d_- = d$. The valences for anions and counterions are defined by Z_- and Z_+, respectively. For simplicity, the counterions of colloidal particles are taken as being equal to small ions, such that the charge of the counterions neutralizes the total charge on the macroions. Thus, we can obtain here either more cations than anions or vise versa, depending of the sign of the macroions.

In this model, the interaction between anions and counterions is described by a pairwise additive potential such as $u_{ij}(r) = \frac{e^2 Z_i Z_j}{\epsilon r}$ for $r > d_{ij}$, or $u_{ij}(r) = \infty$ for $r < d_{ij}$, where $d_{ij} = (d_i + d_j)/2$. The macroion–macroion interaction [10, 11, 24–26] becomes $u_{\rm MM}(r) = \frac{e^2 Z_{\rm M} Z_{\rm M}}{\epsilon}\left(\frac{2d_{\rm M} - r}{d_{\rm M}^2}\right)$ for $r < d_{\rm M}$ and $u_{\rm MM}(r) = \frac{e^2 Z_{\rm M} Z_{\rm M}}{\epsilon r}$ for $r > d_{\rm M}$ while the ion–macroion interaction becomes $u_{\rm iM}(r) = \frac{e^2 Z_i Z_{\rm M}}{\epsilon}\left(\frac{2}{d_{\rm M}}\right)$ for $r < d_{\rm M}/2$ and $u_{\rm iM}(r) = \frac{e^2 Z_i Z_{\rm M}}{\epsilon r}$ for $d_{\rm M}/2 < r$.

The density functional approach for classical ionic fluids is known to provide a powerful and well-established framework for investigating on an equal footing the structural and thermodynamic properties such as pressure, thermal compressibility, or bulk phase behavior [1]. In this case, the grand potential $\Omega[\rho_i(\vec{r})]$, which is the functional of $\rho_i(\vec{r})$, is given by

$$\Omega[\rho_i(\vec{r})] = F[\rho_i(\vec{r})] + \sum_{i=+,-,M} \int d\vec{r}\, \rho_i(\vec{r})[u_{{\rm ext},i}(\vec{r}) - \mu_i], \quad (1)$$

where $u_{{\rm ext},i}(\vec{r})$ is an arbitrary external field on species i and μ_i denotes the chemical potential of the particle reservoir of species i. The Helmholtz free energy $F[\rho_i(\vec{r})]$ of a system, which is the functional of ionic density $\rho_i(\vec{r})$, can be written as

$$F[\rho_i(\vec{r})] = F_{\rm id}[\rho_i(\vec{r})] + F_{\rm coul}[\rho_i(\vec{r})] + F_{\rm hs}[\rho_i(\vec{r})] + F_{\rm el}[\rho_i(\vec{r})]. \quad (2)$$

In Eq. (2), $\beta F_{\rm id}[\rho_i(\vec{r})] = \sum_{i=+,-,M} \int d\vec{r} \rho_i(\vec{r})[\ln \rho_i(\vec{r})\Lambda_i^3 - 1]$ is the ideal free energy of the ions corresponding to the kinetic energy of ions, where Λ_i is the thermal de Broglie wavelength of species i, $\beta = 1/k_{\rm B}T$, with $k_{\rm B}$ being the Boltzmann constant and T the temperature. The Coulomb interaction $F_{\rm coul}[\rho_i(\vec{r})]$ between ions that interact with the local charge density becomes $F_{\rm coul}[\rho_i(\vec{r})] = \frac{1}{2}\sum_{i,j=+,-,M} \int d\vec{r} \int d\vec{s}\, \frac{\rho_{{\rm N}i}(\vec{r})\rho_{{\rm N}j}(\vec{s})}{\epsilon|\vec{r}-\vec{s}|}$. For the macroions with charge smeared uniformly on the 'surface', the local charge density $\rho_{\rm NM}(\vec{r})$ is given by

$$\rho_{\rm NM}(\vec{r}) = \frac{eZ_{\rm M}}{\pi d_{\rm M}^2} \int d\vec{s}\, \rho_{\rm M}(\vec{s}) \delta\left(\frac{d_{\rm M}}{2} - |\vec{r} - \vec{s}|\right), \quad (3)$$

where $\delta(x)$ is the delta function. We note that for the small ions with charge embedded at the center of sphere, the local charge densities become $\rho_{\rm N+}(\vec{r}) = eZ_+\rho_+(\vec{r})$ and

$\rho_{\mathrm{N}-}(\vec{r}) = eZ_-\rho_-(\vec{r})$. Thus, for the CPM, where the charge of the macroion is located at its center, the local charge density of the microions simply becomes $\rho_{\mathrm{NM}}(\vec{r}) = eZ_{\mathrm{M}}\rho_{\mathrm{M}}(\vec{r})$. The third term, $F_{\mathrm{hs}}[\rho_i(\vec{r})]$, denotes the hard-sphere contribution between the ions that were assumed to be the hard spheres. We here adopt the modified fundamental-measure theory (MFMT) [27–29], which is known to be a successful for hard-sphere system:

$$\beta F_{\mathrm{hs}}[\rho_i(\vec{r})] = \int \mathrm{d}\vec{r}\, \Phi_{\mathrm{hs}}[n_\alpha(\vec{r})], \tag{4}$$

where $\Phi_{\mathrm{hs}}[n_\alpha(\vec{r})]$ is the excess free energy of the hard-sphere system per volume. The last term, $F_{\mathrm{el}}[\rho_i(\vec{r})]$, is the electronic residual contribution, which corresponds to the cross correlation between the hard-sphere contribution and the Coulomb interaction. We approximate the free energy as

$$\beta F_{\mathrm{el}}[\rho_i(\vec{r})] = -\frac{1}{2}\sum_{i,j=+,-,M}\int \mathrm{d}\vec{r}\int \mathrm{d}\vec{s}\, c^{(2)}_{\mathrm{el},ij}(|\vec{r}-\vec{s}|,\rho_i)\rho_i(\vec{r})\rho_j(\vec{s}), \tag{5}$$

where $c^{(2)}_{\mathrm{el},ij}(r,\rho_i)$ is the two-particle direct correlation function (DCF) for the electronic residual contribution. An analytic expression for a uniformly charged hard-sphere mixtures based on the MSA solution [30–34] was used to calculate the electronic residual contribution. The detailed expression for $c^{(2)}_{\mathrm{el},ij}(r,\rho_i)$ is presented in the Appendix. We note that the main difference between the CPM and the MCPM is the electronic residual contribution originating from the cross correlation between the Coulomb potential and the hard-sphere interaction of ions.

Because of the charge distribution of the macroions, the microions also interact with the mean electrostatic potential $\psi(\vec{r})$ through

$$\psi_{\mathrm{NM}}(\vec{r}) = \frac{eZ_{\mathrm{M}}}{\pi d_{\mathrm{M}}^2}\int \mathrm{d}\vec{s}\,\psi(\vec{s})\delta\left(\frac{d_{\mathrm{M}}}{2}-|\vec{r}-\vec{s}|\right). \tag{6}$$

We should mention that for small ions with a charge embedded at the center of a sphere, the mean electrostatic potential simply becomes $\psi_{\mathrm{N}+}(\vec{r}) = eZ_+\psi(\vec{r})$ and $\psi_{\mathrm{N}-}(\vec{r}) = eZ_-\psi(\vec{r})$. Then, the Poisson equation for small ions and smeared-out macroions is simply given by

$$\nabla^2\psi(\vec{r}) = -\frac{4\pi}{\epsilon}\sum_{i=+,-} eZ_i\rho_i(\vec{r}) - \frac{4\pi}{\epsilon}\rho_{\mathrm{NM}}(\vec{r}) \tag{7}$$

because $\rho_{\mathrm{N}+}(\vec{r}) = eZ_+\rho_+(\vec{r})$ and $\rho_{\mathrm{N}-}(\vec{r}) = eZ_-\rho_-(\vec{r})$. Finally, the equilibrium ionic density $\rho_i(\vec{r})$ becomes, from the minimization of the grand potential functional $\Omega[\rho_i(\vec{r})]$ with respect to the ionic density $\rho_i(\vec{r})$,

$$\begin{aligned}\ln\left[\frac{\rho_i(\vec{r})}{\rho_i}\right] =& -\beta u_{\mathrm{ext},i}(\vec{r}) - \beta\psi_{\mathrm{N}i}(\vec{r}) - \frac{\delta\beta F_{\mathrm{hs}}[\rho_i(\vec{r})]}{\delta\rho_i(\vec{r})} \\ & - \frac{\delta\beta F_{\mathrm{el}}[\rho_i(\vec{r})]}{\delta\rho_i(\vec{r})} + \frac{\partial\beta F_{\mathrm{hs}}(\rho_i)}{\partial\rho_i} + \frac{\partial\beta F_{\mathrm{el}}(\rho_i)}{\partial\rho_i},\end{aligned} \tag{8}$$

where ρ_i is the bulk ionic density of species i. For the electrolytes near the macroions, the local particle density $\rho_i(\vec{r})$, local charge density $\rho_{\mathrm{NM}}(\vec{r})$, and mean electrostatic potential $\psi_{\mathrm{N}i}(\vec{r})$ depend only on r because of the spherical symmetry; i.e., $\rho_i(\vec{r}) = \rho_i(r)$, $\rho_{\mathrm{NM}}(\vec{r}) = \rho_{\mathrm{NM}}(r)$ and $\psi_{\mathrm{N}i}(\vec{r}) = \psi_{\mathrm{N}i}(r)$. The external potential $\beta u_{\mathrm{ext},i}(r)$ for the central macroion becomes $\beta u_{\mathrm{ext},i}(r) = \infty$ for $r < d_{\mathrm{M}}/2$ and zero otherwise. Then, the equilibrium ionic density $\rho_i(r)$ becomes

$$\begin{aligned}\ln\left[\frac{\rho_i(r)}{\rho_i}\right] =& -\beta\psi_{\mathrm{N}i}(r) - \frac{\delta\beta F_{\mathrm{hs}}[\rho_i(r)]}{\delta\rho_i(r)} - \frac{\delta\beta F_{\mathrm{el}}[\rho_i(r)]}{\delta\rho_i(r)} \\ & + \frac{\partial\beta F_{\mathrm{hs}}(\rho_i)}{\partial\rho_i} + \frac{\partial\beta F_{\mathrm{el}}(\rho_i)}{\partial\rho_i}, \quad r > d_{\mathrm{M}}/2\end{aligned} \tag{9}$$

and zero otherwise. For the CPM model, $\beta\psi_{\mathrm{N}i}(r)$ becomes $\beta\psi_{\mathrm{N}i}(r) = \beta\psi(r)$. The local particle density and the mean electrostatic potential can be found numerically with an iteration procedure, the so-called the standard Picard method, along with the over-all electroneutrality condition $\int_{d_{\mathrm{M}}/2}^{\infty}\mathrm{d}\vec{r}\left[\sum_{i=+,-} eZ_i\rho_i(\vec{r}) + \rho_{\mathrm{NM}}(\vec{r})\right] + \pi d_{\mathrm{M}}^2\sigma_{\mathrm{M}} = 0$.

On the other hand, the potential of the mean force for each species i contains contributions from the electrostatic and the hard-sphere correlations. The potential of the mean force between the central macroion and the other species in the electrolytes can be obtained from Eq. (8) as

$$w_i(r) = -k_{\mathrm{B}}T\ln[\rho_i(r)/\rho_i] = \psi_{\mathrm{N}i}(r) + J_i(r), \quad r > d_{\mathrm{M}}/2, \tag{10}$$

where $J_i(r)$ is the entropic potential; i.e., $J_i(r) = \frac{\delta F_{\mathrm{hs}}[\rho_i(\vec{r})]}{\delta\rho_i(\vec{r})} + \frac{\delta F_{\mathrm{el}}[\rho_i(\vec{r})]}{\delta\rho_i(\vec{r})} - \frac{\partial F_{\mathrm{hs}}(\rho_i)}{\partial\rho_i} - \frac{\partial F_{\mathrm{el}}(\rho_i)}{\partial\rho_i}$ [19, 20]. Energetic or entropic competition takes place between different ionic components in the colloidal dispersions. The mean force $F_{w_i}(r) = -\frac{\mathrm{d}w_i(r)}{\mathrm{d}r}$ is proportional to the electrostatic and entropic components as

$$F_{wi}(r) = F_{ei}(r) + F_{si}(r), \tag{11}$$

where the electrostatic component becomes $F_{ei}(r) = -\frac{\mathrm{d}\psi_{\mathrm{N}i}(r)}{\mathrm{d}r}$, which is just the derivative of $\psi_{\mathrm{N}i}(r)$ with respect to r. The entropic component becomes $F_{si}(r) = -\frac{\mathrm{d}J_i(r)}{\mathrm{d}r}$. Both components are functionals of the local particle densities, $\rho_i(r)$, implying that the size correlations are coupled. Thus, the (total) mean force between the central macroion and an ion of species i becomes

$$F_{\mathrm{M}i}(r) = \frac{1}{\beta}\frac{\mathrm{d}}{\mathrm{d}r}\left[\ln\left(\frac{\rho_i(r)}{\rho_i}\right)\right] = \frac{1}{\beta}\frac{\mathrm{d}}{\mathrm{d}r}\left[\ln g_{\mathrm{M}i}(r)\right], \quad r > d_{\mathrm{M}}/2, \tag{12}$$

where $g_{\mathrm{M}i}(r) = \rho_i(r)/\rho_i$ is the radial distribution function between the central macroion and an ion of species i.

3 Results and discussion

In the CPM and the MCPM, the solvent is modelled as uniform dielectric continuum characterized by its dielectric constant $\epsilon = 78.5$ at temperature $T = 298$ K so that the results can be compared with available simulation data [21]. In all cases, the added salt is a 1:1, 0.1 M electrolyte with ionic diameter $d_+ = d_- = d = 0.425$ nm. The diameter of the macroion is taken to be $d_{\mathrm{M}} = 10\,d$, if not pointed out otherwise. The ionic diameter d is used as a unit length. Both the electrolyte ions and the macroions are assumed to have the same dielectric constant to avoid image charges. Recall that both models, which are the CPM and MCPM, become the restricted primitive model (RPM) in the limit $\phi \to 0$, where $\phi = \pi\rho_{\mathrm{M}}d_{\mathrm{M}}^3/6$ is the packing fraction of the macroions [1–3].

To illustrate the applicability of the present theory, we have calculated the normalized induced charge $Q_{\mathrm{M}}(r)/Q_{\mathrm{M}}$ for the CPM and compared the results with the simulation data [21] in the inset of Fig. 1, where the packing fraction of the macroions is $\phi = 0.24$. The induced charge $Q_{\mathrm{M}}(r)$ around the central macroion, representing the oscillating behavior of the surface charge, is defined by,

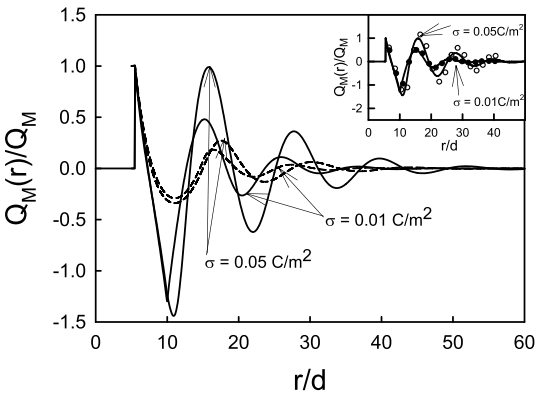

Fig. 1 Normalized induced charge $Q_{\mathrm{M}}(r)/Q_{\mathrm{M}}$ of the CPM (solid line) and the MCPM (dashed line) for the surface charge densities $\sigma = 0.01\,\mathrm{C/m^2}$ and $0.05\,\mathrm{C/m^2}$, where $\phi = 0.24$. The calculated $Q_{\mathrm{M}}(r)/Q_{\mathrm{M}}$ for the CPM is compared with the MC simulations [19] in the inset: solid circles for $\sigma = 0.01\,\mathrm{C/m^2}$ and open circles for $\sigma = 0.05\,\mathrm{C/m^2}$

$$Q_{\mathrm{M}}(r) = Q_{\mathrm{M}} + 4\pi\int_{d_{\mathrm{M}}/2}^{r}\mathrm{d}r\,r^2\left[\sum_{i=+,-}eZ_i\rho_i(r) + \rho_{\mathrm{NM}}(r)\right], \tag{13}$$

where $Q_{\mathrm{M}} = eZ_{\mathrm{M}}$ is the charge on the macroion's surface [21]. In this case, the macroion has $\rho_{\mathrm{M}} = 6\phi/\pi d_{\mathrm{M}}^3 = 9.915\times10^{-3}$ M, equivalent to a macroion packing fraction of $\phi = 0.24$ and a macroion valence of $Z_{\mathrm{M}} = \sigma\pi d_{\mathrm{M}}^2/e = 17.73$, equivalent to a surface charge density $\sigma = 0.05\,\mathrm{C/m^2}$ and $\rho_- = -(Z_+\rho_+ + Z_{\mathrm{M}}\rho_{\mathrm{M}})/Z_- = 0.6286$ M because the negative ions are the sum of the salt anions plus the macroions' counterions. Hence, $Q_{\mathrm{M}}(r)/Q_{\mathrm{M}} = 1$ at the surface of the central macroion, and $Q_{\mathrm{M}}(r)/Q_{\mathrm{M}} \to 0$ when $r \to \infty$ because $Q_{\mathrm{M}}(r \to \infty) \to 0$. Charge reversal occurs when the integrated surface charge displays an opposite sign regarding the sign of the macroion's charge, i.e., $Q_{\mathrm{M}}(r)/Q_{\mathrm{M}} < 0$. On the other hand, the induced charge $Q_{\mathrm{M}}(r)$ is related to the integrated total charge density distribution around the central macroion, which is defined by $\sigma(r) = \frac{\sigma d_{\mathrm{M}}^2}{4r^2} + \frac{1}{r^2}\int_{d_{\mathrm{M}}/2}^{r}\mathrm{d}r\,r^2\left[\sum_{i=+,-}eZ_i\rho_i(r) + \rho_{\mathrm{NM}}(r)\right]$, where σ denotes the surface charge density of a macroion. By Gauss' law the electric field $E_{\mathrm{M}}(r)$ at a distance from the surface of the central macroion is $E_{\mathrm{M}}(r) = 4\pi\sigma(r)/\epsilon$ for $r > d_{\mathrm{M}}/2$. One can see from the insert of Fig. 1 that the CPM, the present theory, which is based on the MSA for the correlation between the hard-sphere contribution and Coulomb interaction, explains the charge reversal and overcharging predicted by the computer simulation, does the HNC/MSA theory of Manzanilla-Granados et al. [19], even though we did not display the results of the HNC/MSA theory in the figure. However, the agreement with the computer simulation slightly deteriorates with increasing surface charge density of the macroion. We think that this disagreement perhaps comes from the basic problem of the MFMT for large-size asymmetric ions at high bulk density. The calculated normalized induced charges $Q_{\mathrm{M}}(r)/Q_{\mathrm{M}}$ for the CPM and the MCPM are compared in Fig. 1. Notice here that $Q_{\mathrm{M}}(r)$ for the MCPM is defined for $r \geq d_{\mathrm{M}}/2$ whereas $Q_{\mathrm{M}}(r)$ for the CPM is defined for $r \geq (d_{\mathrm{M}} + d)/2$ because $\rho_i(r) = 0$ for $r < (d_{\mathrm{M}} + d)/2$. The CPM and the MCPM illustrate that long-range overcharging and charge reversal, which are different from the usual overcharging and charge reversal based on the so-called Stern layer [2–4], occur at a finite fraction of macroions. Recall that the overcharging event is universally driven by the ion size-asymmetric effect [2–4]. The charge oscillations for the CPM and the MCPM are mild at low macroion charge ($\sigma = 0.01\,\mathrm{C/m^2}$). The MCPM predicts milder charge oscillation than the CPM because of the weak electronic residual contribution $F_{\mathrm{el}}[\rho_i(\vec{r})]$. The charge oscillation is directly related to the mean electrostatic potential $\psi(r)$ or $\psi_{\mathrm{N}i}(r)$. Thus, the CPM predicts a stronger more

long-range mean electrostatic potential compared with the MCPM. On the other hand, the CPM and the MCPM show strong charge reversal at $r \approx d_M$, which corresponds to the diameter of the macroion, because of the large concentration of negative ions near the macroions. However, the charge oscillations for the MCPM decay more rapidly than those for the CPM. The above result contradicts that of Manzanilla-Granados et al. [20] for the MCPM; the CPM and the MCPM, which are based on the HNC/MSA model, predict the same particle distribution functions and mean forces between macroions. They predicted that the CPM had a much smoother, short-range correlation than of the MCPM. In our calculation, the first peak for the CPM was observed at $r \approx 3d_M/2$ whereas the first peak for the MCPM was found at some distance away from $r \approx 3d_M/2$, even though the charge correlation increased with increasing surface charge density of macroions. We observed the long-range charge reversal at $r \approx d_M$ to be a magnitude higher in absolute value than the original surface charge of a macroion. This result confirms that the charge distribution of macroions is affected by the charge correlation in a colloidal suspension.

The calculated normalized induced charges $Q_M(r)/Q_M$ for the CPM and the MCPM are presented in Fig. 2, where the surface charge densities are $\sigma = 0.05\,C/m^2$ and $\sigma = 0.10\,C/m^2$ and the packing fraction of macroions is $\phi = 0.12$. As can be expected from Fig. 1, the charge oscillations are mild at a low surface charge density ($\sigma = 0.05\,C/m^2$) rather than a high surface charge density ($\sigma = 0.10\,C/m^2$). The reader should note that the valence Z_M of macroions increases with increasing surface charge density σ of macroions because $Z_M = \sigma\pi d_M^2/e$ and that the packing fraction of negative ions ρ_- also increases to satisfy electroneutrality. At the same packing fraction ϕ and surface charge density σ of macroions, a strong, long-range charge oscillation is found when using the CPM rather than the MCPM because of the strong electronic residual contribution $F_{el}[\rho_i(\vec{r})]$.

Figure 3 depicts the radial distribution functions for the macroions, $g_{MM} = \rho_M(r)/\rho_M$, for the MCPM and the CPM, where the surface charge densities are $\sigma = 0.05\,C/m^2$ and $\sigma = 0.10\,C/m^2$, and $\phi = 0.12$. Here, the radial distribution functions for the negative and the positive ions, g_{M-} and g_{M+}, are defined as $g_{M-} = \rho_-(r)/\rho_-$ and $g_{M+} = \rho_+(r)/\rho_+$, respectively, because a macroion has been chosen as the central ion. The peaks of the radial distribution functions for the CPM and the MCPM appear at $r \approx 7d_M/5$, and the charge oscillation attenuates very fast for the low surface-charge density ($\sigma = 0.05\,C/m^2$). The radial distribution function $g_{MM}(r)$ for the MCPM also shows a long-range correlation, even though the CPM predicts a slightly higher particle density distribution than the MCPM. This result implies that the particle density distributions of positive and negative ions are strongly affected by the particle density distribution of macroions. The inset of Fig. 3 shows the local charge density $\rho_{NM}(r)$ of macroions, where $\rho_{NM}(\vec{r}) = \frac{eZ_M}{\pi d_M^2}\int d\vec{s}\,\rho_M(\vec{s})\delta\left(\frac{d_M}{2} - |\vec{r}-\vec{s}|\right)$. An interesting thing is that the local charge distribution $\rho_{NM}(r)$ for the CPM predicts a maximum at $r \approx d_M$ because $\rho_{MM}(r) = \rho_M(r)$ (see Fig. 3) whereas $\rho_{NM}(r)$ for the MCPM shows a maximum at some distance away from $r = 3d_M/2$ because of the smeared-out macroion (see the insert of Fig. 3). The overall picture illustrates that the particle density distribution of macroions $\rho_M(r)$ depends on the local charge density of macroions, which differs from the results of Manzanilla-Granados et al. [20].

The radial distribution function $g_{Mi}(r)$ obtained from the MCPM for a packing fraction of macroion of $\phi = 0.12$ is displayed in Fig. 4. At a fixed ϕ-value, the high surface

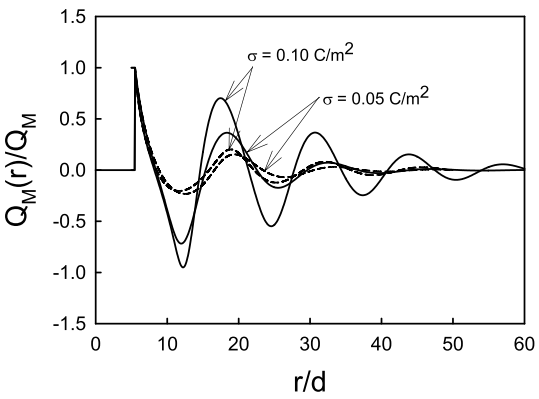

Fig. 2 Normalized induced charge $Q_M(r)/Q_M$ of the CPM (solid line) and the MCPM (dashed line) for a packing fraction $\phi = 0.12$

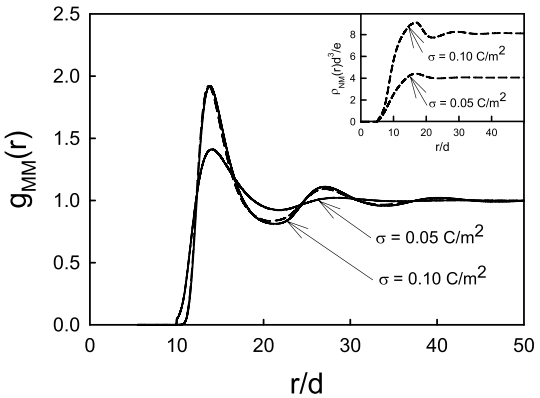

Fig. 3 Radial distribution function $g_{MM} = \rho_M(r)/\rho_M$ for $\phi = 0.12$ and for $\sigma = 0.05\,C/m^2$ or $0.10\,C/m^2$. The solid and the dashed line represent the CPM and the MCPM, respectively. The inset shows the corresponding local charge density $\rho_{NM}(r)$ for the MCPM. Notice here that the CPM and the MCPM for $\sigma = 0.05\,C/m^2$ are indistinguishable

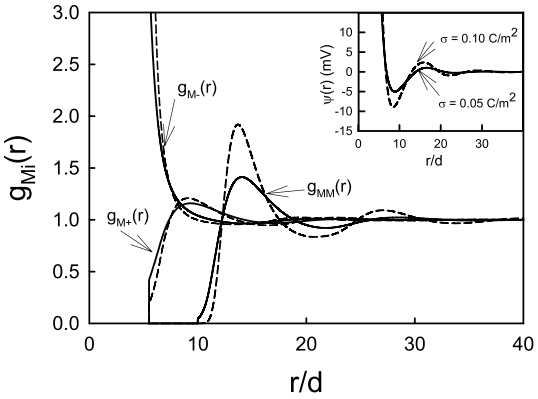

Fig. 4 Radial distribution functions $g_{M-}(r)$, $g_{M+}(r)$ and $g_{MM}(r)$ for the MCPM for a packing fraction of $\phi = 0.12$. The inset shows the mean electrostatic potential $\psi(r)$. The solid and the dashed lines are for $\sigma = 0.05\,\mathrm{C/m^2}$ and $0.10\,\mathrm{C/m^2}$, respectively

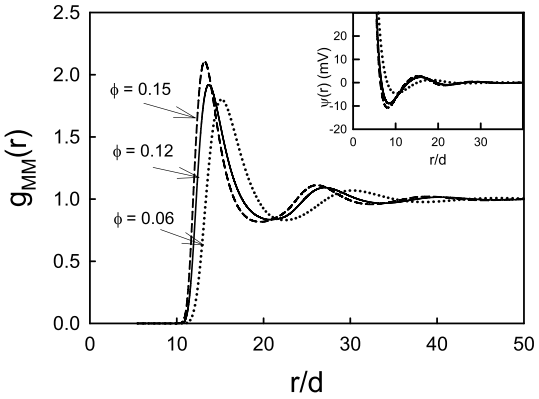

Fig. 5 Radial distribution function $g_{MM}(r)$ for the MCPM where $\sigma = 0.10\,\mathrm{C/m^2}$. The inset shows the mean electrostatic potential $\psi(r)$. The dotted, solid, and dashed lines are for $\phi = 0.06$, 0.12, and 0.15, respectively

charge density implies a high valence for a macroion. Long-range correlations for the mean electrostatic potential. Induced charge appeared for higher surface charge density. At a fixed ϕ-value, the maximum position of $g_{MM}(r)$ comes closer to the central macroion as the surface charge density of macroions increases [21]. This result can be explained as follows: with increasing surface charge of a macroion, the macroions keep away from one another because of the higher repulsive Coulomb force whereas the negative ions, i.e., counterions, $g_{M-}(r)$ accumulates more near the macroion. Thus, a higher particle density of macroions at $r \approx d_M$ appears at a lower surface charge density, and the maximum position of $g_{MM}(r)$ becomes closer to the central macroion as the surface charge of macroion increases. The mean electrostatic potential $\psi(r)$ (see the insert of Fig. 4) also illustrates stronger oscillating behaviors for the CPM than for the MCPM.

Figure 5 shows the radial distribution function $g_{MM}(r)$ for the MCPM, where the surface charge density $\sigma = 0.10\,\mathrm{C/m^2}$. As can be expected from Fig. 4, a increase in the packing fraction of macroions relatively reduces the packing fraction of counterions $\rho_-(r)$. The maximum position of the particle density distribution of macroion becomes closer to the central macroion because an increase in the packing fraction of macroion relatively reduces the available volume of ions. In this case, the entropic force overcomes the repulsive coulomb force. Thus, for a low ϕ-value, $g_{MM}(r)$ attenuates very fast with increasing distance between macroions. Once again, the mean electrostatic potential $\psi(r)$ also shows strong oscillating behaviors at high packing fractions of macroion.

The normalized induced charge $Q_M(r)/Q_M$ for the MCPM is depicted in Fig. 6, where the surface charge density of macroion is $\sigma = 0.10\,\mathrm{C/m^2}$. At a fixed surface charge density ($\sigma = 0.10\,\mathrm{C/m^2}$), the normalized induced charge shows a strong oscillating behavior when the packing fraction of macroion is high ($\phi = 0.15$). The distance between two $Q_M(r)/Q_M$ peaks increases with decreasing packing fraction of macroions. On the other hand, at very high packing fraction of macroions, the distance between two peaks of induced charge is expected to approach the diameter of the macroion. At a high packing fraction of macroions, the model colloidal dispersion shows very long-range charge correlation, as well as charge reversal and overcharging.

The mean forces $F_{MM}(r)d/k_BT$ between two macroions for two different surface charge densities of macroion $\sigma = 0.01\,\mathrm{C/m^2}$ and $\sigma = 0.05\,\mathrm{C/m^2}$ are presented in Fig. 7, where the packing fraction of macroions is $\phi = 0.24$. The (total) mean force between two macroions becomes $\beta F_{MM}(r) = \frac{\mathrm{d}}{\mathrm{d}r}\left[\ln g_{MM}(r)\right]$, where $g_{MM}(r) = \rho_M(r)/\rho_M$ is the radial distribution function of macroions. As can be expected from Fig. 1, at low surface charge density of macroions, the mean force between two macroions near the surface of a macroion is repulsive. At high surface

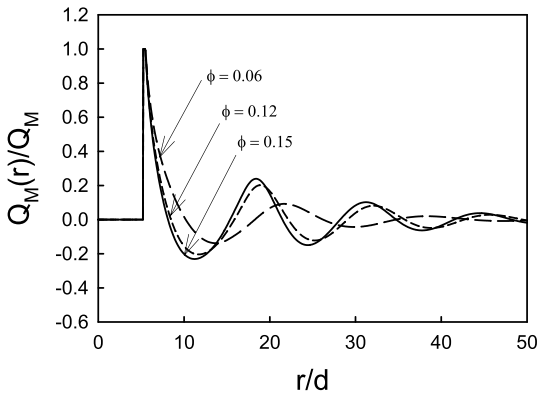

Fig. 6 Normalized induced charge $Q_M(r)/Q_M$ for the MCPM where $\sigma = 0.10\,\mathrm{C/m^2}$. The long-dashed, dashed, and solid lines are for $\phi = 0.06$, 0.12, and 0.15, respectively

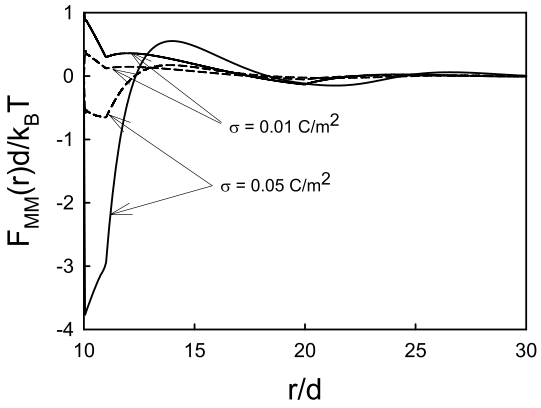

Fig. 7 Mean force $F_{\mathrm{MM}}(r)d/k_{\mathrm{B}}T$ between two macroions for the CPM(solid line) and the MCPM(dashed line), where $\phi = 0.24$

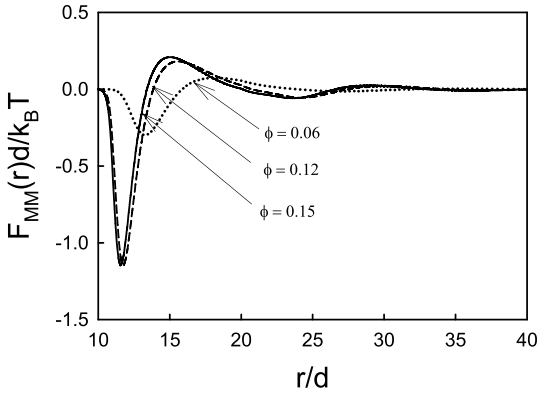

Fig. 8 Mean force $F_{\mathrm{MM}}(r)d/k_{\mathrm{B}}T$ between two macroions for the MCPM, where $\sigma = 0.10\,\mathrm{C/m^2}$. The dotted, dashed, and solid lines are for $\phi = 0.06$, 0.12, and 0.15, respectively

charge density ($\sigma = 0.05\,\mathrm{C/m^2}$), the mean force shows a strong oscillating behavior due to the attractive force at the surface of the macroion and the repulsive force at $r \approx 1.5d_{\mathrm{M}}$. A relatively strong long-range attraction for the highly charged particles was shown experimentally by Ise et al. [6]. The attraction at $r \approx 1.1\,d_{\mathrm{M}}$ comes from the depletion effect due to the negative ions that condensed near the central macroion. Thus, a strong attraction is predicted at high surface charge density of macroions because many negative ions near the central macroion condense. This means that the increase in the surface charge density σ enhances the mean force which has two component: the electrostatic and the entropic forces. The long-range attractions and repulsions are entropic effects, which overcome the electrostatic repulsion of the macroions. Thus, the CPM, in which the colloidal charge is assumed to be in the center of particle, shows a very long-range mean force compared with the MCPM because of the strong electrostatic energy between macroions.

The mean forces between two macroions for the MCPM are displayed in Fig. 8 for $\sigma = 0.10\,\mathrm{C/m^2}$. As can be seen from Fig. 7, the mean force near the surface of a macroion depends strongly on the surface charge density of the macroion σ. At a fixed surface charge density ($\sigma = 0.10\,\mathrm{C/m^2}$), the mean force at the surface of a macroion $r = d_{\mathrm{M}}$ is $g_{\mathrm{MM}}(r = d_{\mathrm{M}}) \approx 0.0$, and a strongly oscillating mean force behavior for a high packing fraction of macroion ($\phi = 0.15$) compared with a low packing fraction ($\phi = 0.06$) is predicted. The attraction at $r \approx 1.2\,d_{\mathrm{M}}$ comes from the effect of the negative ions that condensed near the central macroion. The condensation of negative ions near the central macroion enhances with increasing packing fraction of macroions. The strong attraction at $r \approx 1.2\,d_{\mathrm{M}}$ was predicted at a high packing fraction of macroions. This result explains that the long-range attractions and repulsions in the colloidal dispersion are entropic effects, which overcome the electrostatic repulsion of the macroions. On the other hand, one can calculate the mean force between a macroion and an ion of species i as $\beta F_{\mathrm{M}i}(r) = \frac{\mathrm{d}}{\mathrm{d}r}\left[\ln g_{\mathrm{M}i}(r)\right]$. The mean force is strongly related to the surface charge density of macroions, as well as the packing fraction of macroions. In this case, the mean force $F_{\mathrm{M-}}(r)$ between the macroion and a negative ion is highly attractive at the surface of the macroion whereas the mean force $F_{\mathrm{M+}}(r)$ between the macroion and a positive ion is predicted to be repulsive force (see Fig. 4).

4 Concluding remarks

In this paper, we proposed a theoretical model for studying the structural and the electrostatic properties of uniformly charged ions by using the MCPM. The charge distribution of macroions, which was neglected in the HNC/MSA theory of González-Calderón et al. [20–22], is included in the present theory for satisfying self-consistency in itself. The calculated result implies that the charge distribution of macroions and the packing fraction of macroion are strongly affected by the charge correlations and the mean forces between macroions. This result contradicts those of Manzanilla-Granados et al. [20], where the particle distribution function and the mean force between macroions do not depend on the charge distribution of macroions. A long-range strong charge oscillation in the model colloidal suspension is found for the CPM, in which the colloidal charge is assumed to be in the center of particle, but not in the MCPM, because of the strong electrostatic energy between macroions. The origin of the long-range attractions and repulsions in the charged colloidal dispersions comes from the entropic effects, which

overcome the electrostatic repulsion of the macroions. Thus, strong attractions and repulsions between macroions are found at high packing fractions of macroion.

On the other hand, the present theory can be easily extended to charged colloidal dispersions with a volume charge distribution, i.e., $\rho_{\rm NM}(\vec{r}) = \frac{6eZ_{\rm M}}{\pi d_{\rm M}^3} \int {\rm d}\vec{s}\, \rho_{\rm M}(\vec{s}) \theta\left(\frac{d_{\rm M}}{2} - |\vec{r} - \vec{s}|\right)$, where $\theta(x)$ is the Heaviside step function. Furthermore, one can apply the present theory for studying the structural and the electrostatic properties of polymer latex solutions in which order-disorder structures coexist [8, 9, 22]. We will investigate these issues in the near future.

Acknowledgements This research was supported by the Basic Science Research Program through the National Research Foundation of Korea (NRF) funded by the Ministry of Education (no. 2019R1A6A3A01090186).

Appendix: Electronic residual contribution $c^{(2)}_{{\rm el},ij}(r, \rho_i)$

We used an analytic expression to calculate the electronic residual contribution based on the solution in the mean-spherical approximation, which yields reasonable accuracy [32–34]. The main difference between the MSA solution for size-asymmetric electrolytes with center–center interactions and the present solution for uniformly charged hard-sphere ions is the Coulomb interaction between two ions [10, 11, 24–26]. In the MSA approach, the two-particle, direct, correlation function (DCF) [32–34] for uniformly charged hard-sphere ions, $c^{(2)}_{{\rm chs},ij}(r, \rho_i)$, can be expressed as a sum of the hard-sphere and the electronic residual contributions:

$$\begin{aligned} c^{(2)}_{{\rm chs},ij}(r, \rho_i) =& c^{(2)}_{{\rm hs},ij}(r, \rho_i) + \frac{\beta e^2 Z_i Z_j}{\epsilon} A_{ij}(r) \theta(d_{ij} - r) \\ &+ \frac{e^2 Z_i Z_j}{r} \theta(r - d_{ij}), \end{aligned} \tag{14}$$

where $d_{ij} = (d_i + d_j)/2$ and $c^{(2)}_{{\rm hs},ij}(r, \rho_i)$ is the two-particle DCF of the Percus–Yevick integral equation for the hard spheres [35, 36]. $\theta(x)$ is the Heaviside step function: $\theta(x) = 1$ for $x > 0$, and $\theta(x) = 0$ for $x < 0$. For the MCPM, the coefficients $A_{ij}(r)$ becomes

$$\begin{aligned} A_{ij}(r, \rho_i) &= \alpha_{ij} - Z_i Z_j / r, && 0 \le r \le |d_i - d_j|/2 \\ &= \beta_{ij}/r - Z_i Z_j / r - \gamma_{ij} + r\delta_{ij} + r^3 \xi_{ij}, && |d_i - d_j|/2 \le r \le d_{ij} \\ &= 0, && r > d_{ij} \end{aligned} \tag{15}$$

with

$$\alpha_{ij} = -2[-Z_i n_j + x_i s_j - a_i s_j^2/3], \tag{16}$$

$$\begin{aligned} \beta_{ij} =& (d_i - d_j)[(x_i + x_j)(s_i - s_j)/4 \\ &- (a_i - a_j)[(s_i + s_j)^2 - 4 n_i n_j]/16], \end{aligned} \tag{17}$$

$$\begin{aligned} \gamma_{ij} =& (x_i - x_j)(n_i - n_j) + (x_i^2 + x_j^2)\Gamma \\ &+ (a_i + a_j) n_i n_j - (a_i s_j^2 + a_i s_j^2)/3, \end{aligned} \tag{18}$$

$$\delta_{ij} = x_i s_i / a_i + x_j s_j / a_j + n_i n_j - (s_i^2 + s_j^2)/2, \tag{19}$$

$$\xi_{ij} = [(s_i/a_i)^2 + (s_j/a_j)^2]/6, \tag{20}$$

where $s_i = n_i + \Gamma x_i$ and $x_i = Z_i + n_i d_i$ [34]. The Γ and the n_i functions are obtained numerically to satisfy the algebraic equations

$$\begin{aligned} \Gamma^2 =& \frac{\beta \pi e^2}{\epsilon} \sum_{i=+,-,M} \rho_i (Z_i + n_i d_i)^2 \quad \text{and} \\ &- x_i \Gamma = n_i + c\, d_i \sum_{i=+,-,M} \rho_i d_i x_i \end{aligned} \tag{21}$$

with $c = (\pi/2)[1 - \pi/6 \sum_{i=+,-,M} \rho_i d_i^3]^{-1}$.

The interaction between two charged hard-sphere ions for overlapping separation $u_{ij}(r)$ is given by [10, 11, 26]

$$u_{ij}(r) = \frac{e^2 Z_i Z_j}{\epsilon} B_{ij}(r) \theta(d_{ij} - r) + \frac{e^2 Z_i Z_j}{r} \theta(r - d_{ij}), \tag{22}$$

where the function $B_{ij}(r)$, which represents the interaction potential between the ions [10, 11, 24–26], i.e., the macroion–macroion, macroion–ion, and ion–ion interactions, is simply given by

$$\begin{aligned} B_{\rm MM}(r) =& \frac{2d_{\rm M} - r}{d_{\rm M}^2}, \quad 0 \le r \le d_{\rm M} \\ B_{-+} =& B_{++} = B_{--} = \frac{1}{r}, \quad 0 \le r \le d \\ B_{-M} = B_{+M} =& \frac{2}{d_{\rm M}}, \quad 0 \le r \le d_{\rm M}/2 \\ =& \frac{1}{r}, \quad d_{\rm M}/2 \le r \le (d + d_{\rm M})/2. \end{aligned} \tag{23}$$

Then, the electronic residual contribution between the hard-sphere contribution and the Coulomb interaction $c^{(2)}_{{\rm el},ij}(r, \rho_i)$ becomes

$$\begin{aligned} c^{(2)}_{{\rm el},ij}(r, \rho_i) =& c^{(2)}_{{\rm chs},ij}(r, \rho_i) - c^{(2)}_{{\rm hs},ij}(r, \rho_i) + \beta u_{ij}(r) \\ =& -\frac{\beta e^2 Z_i Z_j}{\epsilon} \Big[A_{ij}(r) + B_{ij}(r) \Big] \theta(d_{ij} - r). \end{aligned} \tag{24}$$

Notice here that for hard-sphere ions with a charge embedded at the center of the sphere (CPM), Eq. (24) exactly

recovers the MSA result for size-asymmetric electrolytes, is derived by Blum and Hiroike [32–34].

References

1. J.-P. Hansen, I.R. McDonald, *Theory of Simple Liquids*, 3rd edn. (Academic Press, London, 2006)
2. S.L. Carnie, G.M. Torrie, Adv. Chem. Phys. **56**, 141 (1984)
3. P. Attard, Adv. Chem. Phys. **92**, 1 (1996)
4. Y. Levin, Rep. Prog. Phys. **65**, 1577 (2002)
5. R.H. Ottewill, Langmuir **5**, 4 (1989)
6. N. Ise, T. Okubo, M. Sugimura, K. Ito, H.J. Nolte, J. Chem. Phys. **78**, 536 (1983)
7. N. Ise, M.V. Smalley, Phys. Rev. B **50**, 16722 (1994)
8. B.V.R. Tata, P.S. Mohanty, M.C. Valsakumara, Solid State Commun. **147**, 360 (2008)
9. P.A. Rundquist, S. Jagannathan, R. Kesavamoorthy, C. Brnardic, S. Xu, S.A. Asher, J. Chem. Phys. **94**, 711 (1991)
10. D. Frydel, Y. Levin, J. Chem. Phys. **138**, 174901 (2013)
11. D. Frydel, J. Chem. Phys. **145**, 184703 (2016)
12. K. Bohinc, G.V. Bossa, S. Gavryushov, S. May, J. Chem. Phys. **145**, 234901 (2016)
13. M. Hatlo, K. Bohinc, L. Lue, J. Chem. Phys. **132**, 114102 (2010)
14. K. Bohinc, J. Grime, L. Lue, Soft Matter **8**, 5679 (2012)
15. K. Bohinc, J. Rescic, L. Lue, Soft Matter **12**, 4397 (2016)
16. S. Spada, S. Gavryushov, K. Bohinc, J. Mol. Liq. **270**, 178 (2018)
17. S. Jang, G.R. Shin, S.-C. Kim, J. Chem. Phys. **147**, 036101 (2017)
18. S. Jang, G.R. Shin, S.-C. Kim, J. Korean Phys. Soc. **74**, 30 (2019)
19. H.M. Manzanilla-Granados, F. Jiménez-ángeles, M. Lozada-Cassou, J. Phys. Chem. B **115**, 12094 (2011)
20. H.M. Manzanilla-Granados, M. Lozada-Cassou, J. Phys. Chem. B **117**, 11812 (2013)
21. A. González-Calderón, M. Chávez-Páez, E. González-Tovar, M. Lozada-Cassou, J. Phys. Chem. B **122**, 7002 (2018)
22. A. González-Calderón, E. González-Tovar, M. Lozada-Cassou, The European Physical Journal Special Topics **227**, 2375 (2019)
23. M. Heo, G.R. Shin, S.-C. Kim, J. Stat. Mech. Theory and Experiment, **P083207** (2019)
24. Y. Rosenfeld, Phys. Rev. A **35**, 938 (1987)
25. J. Stein, D. Shalitin, Y. Rosenfeld, Phys. Rev. A **37**, 4854 (1988)
26. A.R. Denton, Phys. Rev. E **67**, 011804 (2003)
27. R. Roth, R. Evans, A. Lang, G.J. Kahl, J. Phys. Condens. Matter **14**, 12063 (2002)
28. Y. Yu, J. Wu, J. Chem. Phys. **117**, 10156 (2002)
29. Y. Yu, J. Wu, J. Chem. Phys. **118**, 3835 (2003)
30. E. Waisman, J.L. Lebowitz, J. Chem. Phys. **56**, 3086 (1972)
31. G. Rickayzen, Mol. Phys. **97**, 721 (2011)
32. L. Blum, Mol. Phys. **30**, 1529 (1975)
33. L. Blum, J.S. Høye, J. Phys. Chem. **81**, 1311 (1977)
34. K. Hiroike, Mol. Phys. **33**, 1195 (1977)
35. M.S. Wertheim, Phys. Rev. Lett. **10**, 321 (1963)
36. E. Thiele, J. Chem. Phys. **38**, 1959 (1963)